J. Indian Inst. Sci., Nov.–Dec. 2000, **80**, 619–653.
© Indian Institute of Science

IISc THESES ABSTRACTS

Thesis Abstract (Ph. D.)

Uracil DNA glycosylase from mycobacteria and *Escherichia coli*: mechanism of uracil excision from synthetic substrates and differential interaction with uracil DNA glycosylase inhibitor (Ugi) and single stranded DNA binding proteins (SSBs) by Purnapate Kedar Padmakar
Research supervisor: Prof. Umesh Varshney
Department: Microbiology and Cell Biology

1. Introduction

Mycobacteria are responsible for a variety of public health problems. According to recent WHO reports, about 3 million people die every year due to tuberculosis making it the most serious pathogen of the human race. Further, the emergence of multidrug resistant strains has made it imperative to understand the biology of these organisms. Mycobacteria multiply inside the host macrophages where they are subjected to oxidative and other kinds of physiological stresses. Such adverse conditions result in various DNA damages. However, the mechanisms of DNA repair in these organisms have not been studied in detail. (A brief review of current research on mycobacteria, DNA damage and repair in prokaryotes along with DNA repair genes in *M. tuberculosis* is given in Chapter 1 of the thesis).

We are interested in studying the uracil excision repair pathway in mycobacteria. Uracil residues can be incorporated in DNA by DNA polymerase or arise by spontaneous deamination of cytosines. Uracil DNA glycosylase (UDG) excises uracil residues and initiates DNA repair to restore the genetic information. Mycobacteria are at an increased risk of cytosine deamination because of their G + C rich genomes (up to 70%) as well as the unfavourable habitat of the host macrophage where they multiply. Thus, the UDG-mediated DNA repair pathway could be crucial in maintaining the genomic integrity of mycobacteria. In fact, our preliminary studies with cell-free extracts of *E. coli* (50% G + C), *M. smegmatis* (70% G+C), and *M. tuberculosis* (65% G + C) indicated that mycobacteria possess up to 3 fold higher UDG activity.

2. Experimental, results and discussion

In order to study the mechanism of uracil excision in mycobacteria, we have purified UDG from *M. smegmatis* (MsUDG) by more than 3000 fold.[1] A comparative study of uracil excision by *M. smegmatis* and *E. coli* UDG from DNA oligomers of varying lengths, containing uracil in different positions, was performed to determine substrate specificity. Both the UDGs excise uracil from the 5′ terminal position if the oligomers are 5′ phosphorylated but its excision from

the 3′ penultimate position is extremely poor. In agreement with these findings, the minimal substrate for both the UDGs was found to be pd(UN)p. However, the two enzymes differed significantly in their ability to excise uracil from the loop contexts of the DNA hairpin substrates. As reported earlier, excision of uracil from the loop context by EcUDG was highly variable. Interestingly, in the case of MsUDG, the relative efficiency (V_{max}/K_m) of uracil release from various loop substrates differed only by approximately three fold, as opposed to 180 fold difference reported for EcUDG. These results suggest differential interaction of the loop substrates with UDGs. The *M. smegmatis* UDG is most efficient in removal of uracil from various structural contexts and hence can be an enzyme of choice for various applications in molecular biology.

Ugi, a *Bacillus subtilis* PBS2 phage-encoded protein, which shows remarkable electrostatic and shape complementarity with dsDNA inhibits all conserved UDGs by interacting with the substrate-binding site. To study the interaction of MsUDG with Ugi, Ugi gene was cloned from PBS2 genomic DNA into an expression vector pKK 223 and purified. Ugi showed complete inhibition of EcUDG at 1:1 stoichiometry and the EcUDG-Ugi complex was not dissociable under the experimental conditions that we used.[2] However, unlike EcUDG, the MsUDG formed a weak complex with Ugi, which readily dissociated under the same experimental conditions. These differential interactions of the mycobacterial UDGs with the loop substrates and Ugi (substrate mimic) suggest that the amino-acid residues involved in substrate binding are likely to be different in both the enzymes.

The single-stranded DNA-binding protein (SSB) is involved in various DNA functions like replication, repair and recombination. Earlier studies with EcUDG suggested that EcSSB destabilizes the secondary structures in hairpin oligomers and enhances excision of uracil from the first, second or the third position of a tetra loop. However, we observed that inclusion of EcSSB with MsUDG resulted in decreased efficiency of uracil excision from the loop contexts. To further understand the phenomenon of differential effects of EcSSB on EcUDG and MsUDG, we cloned and purified SSB from *M. tuberculosis* (*Mt*SSB), whose complete genome sequence was recently reported.[3] SSB plays an important role in DNA replication, repair and recombination. To study the biochemical properties of SSB from *M. tuberculosis* (*Mt*SSB), we have made use of its recently published genome sequence to clone *ssb* open reading frame by polymerase chain reaction and developed an overexpression system. Sequence comparison reveals that the *Mt*SSB lacks many of the highly conserved amino acids crucial for *Escherichia coli* SSB (*Ec*SSB) structure–function relationship. A highly conserved His55, important for homotetramerization of *Ec*SSB is represented by a Leu in *Mt*SSB. Similarly, Trp40, Trp54 and Trp88 of *Ec*SSB required for stabilizing SSB-DNA complexes are represented by Ile, Phe and Phe, respectively, in *Mt*SSB. Also, a group of positively charged amino acids oriented towards the DNA-binding cleft in *Ec*SSB suffers several nonconserved changes in *Mt*SSB. We show that in spite of these changes in the primary sequence, the *Mt*SSB is similar to *Ec*SSB in its biochemical properties. It exists as a tetramer, has the same minimal size requirement for its efficient binding to DNA and its binding affinity towards DNA oligonucleotides is indistinguishable from that of *Ec*SSB. Further, *Mt*SSB interacts with DNA in at least two distinct modes corresponding to the SSB_{35} and $SSB_{56/65}$ modes of *Ec*SSB interaction with DNA. However, *Mt*SSB does not form heterotetramers with *Ec*SSB. *Mt*SSB, therefore, presents us with an

interesting system to further investigate the role of the conserved amino acids in the biological properties of SSBs.

In this study, the effect of SSBs from *E. coli* (*Ec*SSB) and *M. tuberculosis* (*Mt*SSB) on uracil excision from synthetic substrates by UDGs from *E. coli*, *M. smegmatis* and *M. tuberculosis* (referred to as Ec-, Ms-, and *Mt*UDGs, respectively) has also been investigated. The presence of SSBs with all the three UDGs resulted in decreased efficiency of uracil excision from a single-stranded 'unstructured' oligonucleotide, SS-U9. On the other hand, the addition of EcSSB to EcUDG, or *Mt*SSB to *Mt*UDG reactions resulted in increased efficiency of uracil excision from a hairpin oligonucleotide containing dU at the second position in a tetraloop (Loop-U2). Interestingly, the efficiency of uracil excision by MsUDG from the same substrate was decreased by the presence of either Ec- or *Mt*SSBs. Further, *Mt*SSB also decreased uracil excision from Loop-U2 by *Ec*UDG. Taken together, our studies suggested differential interactions between the two groups (SSBs and UDGs) of the highly conserved proteins. Such studies may provide with important clues to design selective inhibitors against this important class of DNA repair enzymes.[4]

*Mt*SSB (*Mt*SSBΔC), in which the conserved carboxyl terminal acidic amino acid tail of SSBs implicated in interaction with various proteins *in vivo*, was also constructed. The *Mt*SSBΔC inhibited all three UDGs (i.e. EcUDG, MsUDG and *Mt*UDG). These observations suggest that *Mt*SSBΔC possesses the domain required for SSB–UDG interaction.

3. Conclusion

In the present study, the comparative analysis of various biochemical properties of *E. coli* and mycobacterial UDGs has shown that UDGs interact differentially with (i) loop substrates, (ii) Ugi and (iii) SSBs. These observations suggest structural differences between the EcUDG (a prototype of conserved UDGs) and mycobacterial UDGs, which can be exploited for designing selective inhibitors against *Mt*UDG. Further, the availability of cloned *Mt*UDG will facilitate in the gene knockout experiments to elucidate the role of UDG-mediated DNA repair pathway in *M. tuberculosis*.

References

1. Purnapatre, K. and Varshney, U. — Uracil DNA glycosylase from *Mycobacterium smegmatis* and its distinct biochemical properties, *Eur. J. Biochem.*, 1998, **256**, 580–588.
2. Roy, S., Purnapatre, K., Handa, P., Boyanapalli, M. and Varshney, U. — Use of coupled transcriptional system for consistent overexpression and purification of UDG-Ugi complex and Ugi from *Escherichia coli*, *Prot. Expl Purif.*, 1998, **13**, 155–162.
3. Purnapatre, K. and Varshney, U. — Cloning, overexpression and biochemical characterization of single stranded DNA binding protein from *Mycobacterium tuberculosis*, *Eur. J. Biochem.*, 1999, **264**, 591–598.
4. Purnapatre, K., Handa, P., Venkatesh, J. and Varshney, U. — Differential effects of single stranded DNA binding proteins (SSBs) on Uranil DNA glycosylases (UDGs) from *Escherichia coli* and mycobacteria, *Nucleic Acids Res.*, 1999, **27**, 3487–3492.

Thesis Abstract (Ph. D.)
Performance analysis and scheduling of manufacturing supply chain networks by N. R. Srinivasa Raghavan
Research supervisors: Profs N. Viswanadham and Y. Narahari
Department: Computer Science and Automation

1. Introduction

Manufacturing has gone through successive periods of great changes. New materials, such as plastics, ceramics and composites, new technologies such as computer-aided design, manufacture and inspection, and the Internet, new techniques such as Kanban and just in time, new basis for competition such as cost, quality, time or core-competence have all been at the root of these changes. Currently, global competition, demanding customers, liberalization, regulations on environment, emergence of common markets, disintegration of large states, volatile exchange markets, have made manufacturing a more complex function. Customers want everything: low cost, low defect rates, high performance, on the spot delivery, and maintenance without irritants. To meet such demanding customer needs, computer-aided automation, effective flexibility management, strategic alliances, management of end-to-end business processes such as supply chain process and new product development process are important.

Traditionally, manufacturing systems are viewed as a sequential arrangement of functions such as design, manufacture, R&D, marketing, finance, etc. The recent trend[1] is to view a manufacturing system not in terms of functions, divisions, or products, but as a collection of value-delivering processes. Functional or hierarchical structures typically present responsibilities and reporting relationships whereas process structure is a dynamic view of how the organization delivers value to the customer.

Performance measures are useful to evaluate, control and improve business processes. They can also be used to compare similar processes in different companies for benchmarking purposes. World class companies recognize the importance of metrics in helping to define the goals and performance expectations for the organizations. The performance measures include lead time, quality, flexibility, on time delivery, etc. These process performance measures summarize directly the product and system performances as well as the customer satisfaction levels.

In this work, we approach the performance analysis and scheduling of manufacturing organizations by focusing on the business processes and their interfaces. In the process, we transcend current theory which usually deals with models and measures for the factory floor in isolation, or, at best, the conglomeration of business units of a manufacturer.

2. Thesis contribution

We look at the entire value delivery process starting from raw material procurement till the delivery of product to the end-customer, at an aggregated level. Our approach also takes note of the logistics process and the interfaces between any two elements of the supply chain. Under assumptions of rapid information transfer and presence of appropriate alliances and trading policies, we study the integrated supply chain, transcending the practice of the current theory which emphasizes only individual elements of the supply chain.

The work looks into three important and inter-related problems in integrated supply chain networks.

2.1. *Dynamic models for performance analysis and design*

We present dynamic models of supply chain networks that help in rapid performance analysis of large supply chain networks, leading to their efficient design. The dynamic models are based on Petri nets and queueing networks. The models capture the suppliers, the logistics, and the distributors in an integrated way.

First, we compare two different production planning and control policies, the make-to-stock and the build-to-order systems, using generalized stochastic Petri net (GSPN) models. The investigations reveal interesting insights into the dynamics of supply chains and the trade-offs involved when choosing a production planning and control policy. We also use integrated queueing and Petri net models[2] for solving the decoupling point location problem. The decoupling point in the supply chain is that facility from where all finished products are assembled to confirmed customer orders. All facilities upstream of this point produce material to stock. While deciding on this decoupling point, one has to tradeoff between inventory holding costs and customer order delay costs. We show how the decoupling point shifts along a pipeline type of supply chain when the ratio of the above costs varies.

Next, we present queueing network models for analysis at an aggregated level, for the entire supply chain. We also propose a new method of approximate analysis of a class of fork-join queueing (FJQ) networks relevant for supply chain modeling. Specifically, we consider an FJQ system with deterministic arrivals and normally distributed processing times. Our method makes use of an earlier result on the maximum of n normally distributed random variables to obtain a fast and accurate estimate of the mean waiting time at the fork-join station. We present interesting applications of this analysis in the context of supply chains like setting service levels in a two-echelon make-to-stock supply chain, determining delivery reliability and some logistics ownership decisions.

2.2. *Sequencing and capacity planning*

We formulate and solve the integrated sequencing and rough-cut capacity planning problem for the entire supply chain. The resulting nonlinear programming problem has as objective the weighted sum of squared tardiness and squared earliness of customer orders. Capacity constraints limit the allocation of orders to the facilities, while the product structure required for each customer order is captured by the precedence constraints. We use Lagrangian relaxation to solve the problem. With certain modifications to an existing approach,[3] we show how our method provides an efficient solution to this important problem.

2.3. *Dynamic scheduling*

For dynamic, integrated scheduling of supply chains, we propose the use of innovative scheduling policies called fluctuation smoothing policies,[4] employing the modeling framework of multiclass fork-join queueing networks. These policies are shown to reduce the mean and variance of supply chain lead times appreciably, by means of extensive simulations.

3. Conclusions

This work has made several original and innovative contributions to the area of performance analysis and scheduling of integrated manufacturing supply chain networks. These include:

1. GSPN models and their analysis, for performance evaluation of various inventory control policies.
2. A new approximation approach for analyzing fork-join queueing networks with infinite buffer sizes and no blocking. (Our results here can find applications in numerous other systems that use fork-join primitives, like in computers and communication systems, factory floors, etc.)
3. A new method for solving the customer order decoupling point location problem using integrated queueing and Petri net model.
4. Formulating the static deterministic sequencing for the entire supply chain, and rough-cut capacity planning problem. We use Lagrangian relaxation to solve the resulting constrained nonlinear optimization problem.
5. Applying certain innovative scheduling policies, called the fluctuation smoothing policies (originally applied in the context of re-entrant lines), to the integrated supply chain to reduce the mean and variance of total supply chain lead times.

We consider the integrated supply chain network for modeling, instead of just the factory floor or logistics operations in isolation. The speciality of our models is that we have decomposed the supply chain explaining the various interfaces and incorporated them into all our models.

References

1. VISWANADHAM, N. — *Analysis and design of manufacturing enterprises*, Kluwer, 1999.
2. VISWANADHAM, N. AND NARAHARI, Y. — *Performance modeling of automated manufacturing systems*, Prentice Hall, 1992.
3. CZERWINSKI, C. S. AND LUH, P. B. — Scheduling products with bills of material Lagrangian relaxation technique, *IEEE Trans.*, 1994, **RA-10**, 1–13.
4. KUMAR, P. R. — Scheduling queueing networks: Stability, performance analysis, and design, *Proc. IMA Workshop on Stochastic Networks*, July 1994.

Thesis Abstract (M. Sc. (Engng))

Vibration analysis of randomly parametered frame structures with non-gaussian inhomogeneities using Monte Carlo simulations by Subarna Bhattacharyya
Research supervisor: Dr C. S. Manohar
Department: Civil Engineering

1. Introduction

Vibration analysis of engineering structures having random inhomogeneities in their system properties is an active area in structural mechanics research. A major recent development has

been the generalization of finite-element structural analysis procedures to include the effects of system stochasticity. Research work on these problems carried out in our department over the last few years has resulted in the development of a method to analyse the dynamics of skeletal structures using stochastic dynamic stiffness matrices. The dynamic stiffness coefficients for a general beam element have been developed using variational methods employing frequency-dependent shape functions. Specifically, the objectives of this work are two fold. The first objective encompasses the modeling and simulation of system properties as nongaussian random fields. Parametric studies were carried out to investigate the effect of various nongaussian stochasticities in the system properties on the response statistics of structure using dynamic stiffness matrix methods. Secondly, we explore the field of reliability assessment of simple randomly parametered structures in vibration environment employing advanced Monte Carlo simulation methods like importance sampling techniques. The emphasis here is to compute very low failure probabilities using specialized simulation techniques.

2. Dynamic stiffness coefficients of random beam elements

The direct dynamic stiffness method provides a powerful tool to carry out an exact harmonic stochastic steady-state response analysis of skeletal structures. A generalization of this approach to deal with skeletal structures with stochastic parameter variations has been recently proposed by Manohar and Adhikari[1] and Adhikari and Manohar.[2, 3] The work reported in this paper builds on the earlier works of Manohar and Adhikari and aims to develop strategies to model dynamic stiffness coefficients of a beam element taking into account the nongaussian features of the system property random fields. Towards this end, we begin by considering the harmonic response of an Euler–Bernoulli beam element which rests on an elastic foundation. Issues on modeling of the flexural rigidity, mass density and elastic modulus as nongaussian random fields are considered next. The moments and probability distribution function of the dynamic stiffness coefficients are surveyed by varying models for nongaussian distributions and correlation lengths of the system property random fields. Subsequently, statistics of the forced vibration response spectra are studied for a few skeletal structures using the stochastic dynamic stiffness matrix approach.

3. Governing equations

A 2-dimensional beam element having 4 degrees of freedom is considered in this study. We consider only the flexural deformation of the beam and we assume that the axial forces are too small to affect flexural deformations. The behaviour of the beam is taken to follow the Euler–Bernoulli hypotheses and the beam is taken to rest on Winkler's elastic foundation. The governing field equation of motion under these assumptions is given by

$$\frac{\partial^2}{\partial x^2}\left[EI(x)\frac{\partial^2 Y}{\partial x^2}+c_1 EI(x)\frac{\partial^3 Y}{\partial x^2 \partial t}\right]+m(x)\frac{\partial^2 Y}{\partial t^2}+c_2\frac{\partial Y}{\partial t}+k(x)Y=0.$$

Here, $Y(x, t)$ is transverse flexural displacement, $EI(x)$, flexural rigidity, $m(x)$, mass per unit length, $k(x)$, elastic foundation modulus, c_1, strain rate-dependent viscous damping coefficient and c_2, velocity-dependent viscous damping coefficient. The quantities $k(x)$, $m(x)$, and $EI(x)$ in

this study are modeled as homogeneous random fields having the forms $k(x) = k_0[1 + \varepsilon_1 f_1(x)]$, $m(x) = m_0[1 + \varepsilon_2 f_2(x)]$ and $EI(x) = EI_0[1 + \varepsilon_3 f_3(x)]$, respectively. Here, k_0, m_0 and EI_0 denote, respectively, the mean values of $k(x)$, $m(x)$ and $EI(x)$, $0 < \varepsilon_i << 1$ $(i = 1, 2, 3)$ are deterministic constants and the random fields $f_i(x)$ $(i = 1, 2, 3)$ are taken to be jointly homogeneous with zero mean and have covariance $R_{ij}(\xi)$. The following additional restrictions are taken to apply on the random fields $f_i(x)$ $(i = 1, 2, 3)$: (a) $f_i(x)$ $(i = 1, 2, 3)$ are mean square bounded, (b) $f_3(x)$ is twice differentiable in a mean square sense which in turn requires that $\partial^4 R_{33}(x_1, x_2)/\partial x_1^2 \partial x_2^2$ must exist for all x_1 and x_2 in the interval $(0, L)$ and (c) $f_3(x)$ for a specified deterministic function $g(x)$, which is bounded and continuous in $(0, L)$, integrals of the type $\int_0^L g(x) f_i(x) dx$ exist in a mean square sense; this requires that $\int_0^L \int_0^L |g(x_1) g(x_2) R_{ii}(x_1, x_2)| dx_1 dx_2 < \infty$ $(i = 1, 2, 3)$.

4. Nongaussian random field models for $f_i(x)$, $(i = 1, 2, 3)$

In addition to the smoothness and homogeneity requirements mentioned in the previous section, the random fields $f_i(x)$, $(i = 1, 2, 3)$ also need to satisfy the requirement that $P[1 + \varepsilon f_i(x) \leq 0] = 0$, $(i = 1, 2, 3)$. This follows from the fact that the system properties $EI(x)$, $m(x)$ and $k(x)$ are strictly positive. It is clear that the gaussian models do not satisfy this requirement since a gaussian variate has a range from $-\infty$ to $+\infty$. This drawback can be overcome by adopting strictly positive nongaussian distributions with finite bounds on the random variations. What appears currently practicable is to specify the first-order probability density function and the covariance function. Alternatively, it is still more likely that it may be possible to only deduce bounds on the random fields and to estimate the covariance function.

Let $f(x)$ be a system property random field. We consider the situation in which the range (a, b), mean and the covariance function $R_{ff}(\xi)$ are specified. This information in itself is inadequate to simulate samples of $f(x)$. The least we need to know is the first-order probability density function $p_F(f; x)$ of $f(x)$. In the present problem, maximum entropy principle is used to find out the probability density function of a random variable when all we know about the variable is its mean, variance and bounds. Let m and σ^2 be the mean and variance of $f(x)$, respectively, and let $f(x)$ be bounded between $[a, b]$. We then maximize the entropy function subject to the constraints $\int_a^b p_F(f) \mathrm{d}f = 1$, $\int_a^b f p_F(f) \mathrm{d}f = m$ and $\int_a^b (f - m)^2 p_F(f) \mathrm{d}f = \sigma^2$ and obtain the desired probability density function as

$$p_F(f) = A \exp\left[-\lambda_1 f - \lambda_2 f^2\right], a < f < b.$$

Here, A, λ_1 and λ_2 are the constants to be determined from the constraint equations.

5. Numerical results

Using the above equation for probability density function along with the desired expression for the autocorrelation function, three different models for system property stochasticities agreeing at the mean and covariance level but differing in probability density function have been simulated using existing methods of simulation. The stochastic dynamic stiffness matrix for a general random beam element resting on random elastic foundation has been evaluated. Con-

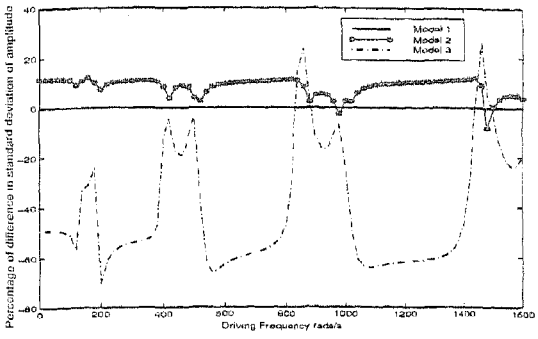

FIG. 1. % difference in standard deviation of amplitude of octahedral shear stress at the midpoint of beam for different pdf models for system property random fields.

sequently, the stochastic dynamic stiffness matrix so obtained has been used to obtain the harmonic steady-state response as well as transient response of a few skeletal structures within the framework of stochastic finite-element method. As an illustration, let us consider the following examples.

We consider a single span-propped cantilever beam resting on an elastic foundation, subjected to a harmonic moment at the propped end. The parameters are as follows: mean mass density, $m_0 = 0.088$ kg/m, mean flexural rigidity, $EI_0 = 0.7787$ Nm^2, mean elastic foundation modulus, $k_0 = 2.7037$ N/m^2, strain rate-dependent viscous damping coefficient, $c_1 = 0.95$ s, length of beam, L = 0.6 m, and magnitude of moment, P = 1.38 Nm. The response variables of interest here are the displacements and octahedral shear stresses. In Fig. 1, the effect of system property nongaussianity on the standard deviations of stresses is shown.

6. Importance of sampling technique in reliability assessment

A preliminary study on the reliability of structures in vibration environment is carried out using adaptive importance sampling technique in conjunction with the stochastic dynamic stiffness matrix approach. However, this study is conducted with random variable models having identical nongaussian probability density functions as before. The method is computationally efficient as is evident from the table of results below. The crossing of a threshold stress level in the first example considered has been taken as the failure criteria and the probability of failure has been evaluated using the above-mentioned technique.

Table 1
Results of adaptive importance sampling for computation of probability of crossing the threshold stress for different random variable models of system stochasticities

$P[T > T^*]$	Model 1 (T^*)	Model 2 (T^*)	Model 3 (T^*)
1.2E-03	0.812E+08	0.824E+08	0.836E+08
4.5E-05	0.900E+08	0.920E+08	0.951E+08
6.7E-07	0.988E+08	1.05E+08	1.236E+08
0.2E-09	1.164E+08	1.609E+08	1.630E+08
9.7E-11	1.340E+08	1.70E+08	1.806E+08
2.36E-12	1.604E+08	2.02E+08	2.31E+08

7. Conclusions

A class of nongaussian models for flexural rigidity, mean density and elastic modulus are proposed based on the principle of maximum entropy. These models are constructed with the knowledge of the range of stochastic variations, mean and covariance function of the random fields. Within the framework of this modeling strategy, it has been possible to construct alternative random field models which possess identical mean and convariance functions. Furthermore, computer programs to generate samples of these random fields have been developed and validated. A procedure for discretizing nongaussian random fields using dynamic weighted integral approach has been proposed. This involves the use of maximum entropy principle in conjunction with elementary principles of interval algebra. The numerical results obtained demonstrate that the differences in first-order probability distribution of the system property random fields is of the same order as that produced by differences in correlation lengths of the system stochastics. This indicates the need for accurate modelling of the auto correlation functions and the first-order probability distributions of the system properties. Advanced Monte Carlo simulation methods such as adaptive importance sampling methods are powerful tools for the estimation of failure probabilities in harmonically vibrating systems. Further studies on these method merit serious considerations. The use of reduced simulation methods with gaussian approximations for dynamic weighted integral lead to acceptable estimations of mean and standard deviations of the response variables.

References

1. MANOHAR, C. S. AND ADHIKARI, S. Dynamic stiffness of randomly parametered beams, *Probabilistic Engng Mech.*, 1998, **13**, 39–51.

2. ADHIKARI, S. AND MANOHAR, C. S. Dynamic analysis of framed structures with statistical uncertainties, *Int. J. Numerical Methods Engng*, 1999, **44**, 1157–1178.

3. ADHIKARI, S. AND MANOHAR, C. S. Transient dynamics of stochastically parametered beams, *J. Engng Mech.*, 2000, **126**, 1131–1140.

Thesis Abstract (M. Sc. (Engng))

Critical cross power spectral density models for earthquake loads on multi-supported structures by Srinivas Chennapragada

Department: Civil Engineering

Research supervisor: Dr M. Sekar

1. Introduction

Earthquake load modeling has remained as an active area of research in the field of earthquake engineering over the last few decades. In the study of earthquake response analysis, structures can be considered as being singly or multisupported. Examples for the first class of structures include chimneys, towers, liquid storage tanks and multistoreyed buildings. In this class of problems, the lateral dimensions of the structure are small in comparison with the characteristic wavelength of seismic waves. Thus, all points of the structure, which are connected to the ground, are taken to be acted upon by the same earthquake ground motions. In the second class

of problems, the structure is supported at distances which are comparable to the characteristic seismic wavelength and consequently the supports suffer differential ground motions. These types of structures can either be land based or they can be parts of a bigger primary system. Examples for land-based structures include long span bridges, large dams, petroleum pipelines and those for secondary systems include stairways, piping networks and multispan rotors. In recent years, it has been shown that resultant response due to multisupport differential support motions can exceed the response in structures with uniform support motions. The treatment of earthquake loads as being spatially varying requires the loads to be modeled as a vector of time histories. Thus description of multisupport excitations requires information, not only on time and frequency content of individual components, but also additional information on phasing and time lag effects of the excitations need to be provided.

2. Present study

The work deals with seismic response analysis of industrial piping systems. The study reported herein is an extension to recent work done in our department.[1–4] We model the piping with an Euler–Bernoulli beam as shown in Fig. 1 which is supported at the two ends through discrete springs and which is acted upon by a pair of differential earthquake ground accelerations $u(t)$ and $v(t)$.

The equation of motion for this system can be shown to be given by

$$EIY''''(x,t)+m\ddot{Y}(x,t)+c\dot{Y}(x,t)=0 \tag{1}$$

with the boundary conditions

$$\begin{aligned} &Y''(0,t)=0 \; Y''(L,t)=0; \\ &EIY'''(0,t)=-k_1[Y(0,t)-u(t)]; \\ &EIY'''(L,t)=k_2[Y(L,t)-v(t)]. \end{aligned} \tag{2}$$

The beam is assumed to be at rest at $t=0$ which would mean that

$$Y(x,0)=0 \text{ and } \dot{Y}(x,0)=0. \tag{3}$$

In the above equations, EI is flexural rigidity, m, the mass per unit length, L, the length of the beam, c, the viscous damping coefficient and k_i ($i=1, 2$) are spring constants. The PSD matrix of the input processes is given by

$$S(\omega)=\begin{bmatrix} S_{uu}(\omega) & S_{uv}(\omega) \\ S_{vu}(\omega) & S_{vv}(\omega) \end{bmatrix}. \tag{4}$$

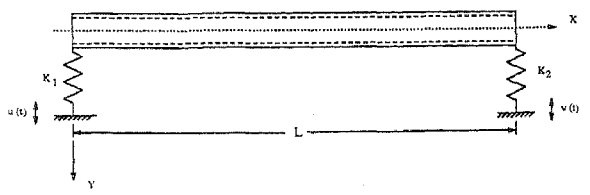

FIG. 1. Piping structure modeled as an Euler–Bernoulli beam with random support motions.

The diagonal terms in this matrix represent the auto-PSD functions while the off-diagonal terms are the cross-PSD functions. The cross-PSD functions are complex valued and they can also be written in the alternative form

$$S_{uv}(\omega) = |S_{uv}(\omega)|\exp\{-i\phi_{uv}(\omega)\} \tag{5}$$

where $\phi_{uv}(\omega)$ is cross phase between input processes. The auto-PSD functions $S_{uu}(\omega)$ and $S_{vv}(\omega)$ for the ground accelerations $\ddot{u}(t)$ and $\ddot{v}(t)$ are taken to be given by the following equations.

$$S_{uu}(\omega) = S_o \frac{\left(1+4\eta_{g1}^2\left(\frac{\omega}{\omega_{g1}}\right)^2\right)}{\left(1-\left(\frac{\omega}{\omega_{g1}}\right)^2\right)^2+\left(4\eta_{g1}^2\left(\frac{\omega}{\omega_{g1}}\right)^2\right)}\left|H_f(\omega)\right|^2; \tag{6}$$

$$S_{vv}(\omega) = S_o \frac{\left(1+4\eta_{g2}^2\left(\frac{\omega}{\omega_{g2}}\right)^2\right)}{\left(1-\left(\frac{\omega}{\omega_{g2}}\right)^2\right)^2+\left(4\eta_{g2}^2\left(\frac{\omega}{\omega_{g2}}\right)^2\right)}\left|H_f(\omega)\right|^2. \tag{7}$$

The filter function $|H_f(\omega)|$ is designed to suppress this undesirable singularity.

3. Nonstationary vector critical random excitation models for linear structures

The support motions are taken to be nonstationary gaussian random processes of the form $\ddot{u}(t) = e_1(t)s_1(t), \ddot{v}(t) = e_2(t)s_2(t)$. Here, $e_1(t)$ and $e_2(t)$ are deterministic envelopes and $s_1(t)$ and $s_2(t)$ are jointly stationary gaussian random processes with auto power spectral density functions $S_{uu}(\omega)$ and $S_{vv}(\omega)$. The deterministic envelope is taken to be $e_1(t) = e_2(t) = e(t) = (\exp(-\gamma_1 t) - \exp(\gamma_2 t))$. The parameters γ_1 and γ_2 in this model control the shape of the enveloping function: thus, for example, with $\gamma_1 = 0.13$ and $\gamma_2 = 0.45$, one gets an earthquake ground motion which lasts for about 30 s and which peaks around 5 s. The governing equation (1) constitutes a homogeneous linear partial differential equation with inhomogeneous time-varying boundary conditions. The traditional solution procedure based on normal mode expansion is not applicable to solve this equation, since the boundary conditions are time varying. Hence, by applying Mindlins and Goodman approach, the solution for the force in the left spring has been produced.

4. Stationary vector critical random excitation models for nonlinear structures

The support motions are $u(t)$ and $v(t)$ are taken to constitute a vector of zero mean, stationary gaussian random processes with psd matrix as given by eqn (4). The springs are taken to be of Duffing type, that is, they possess cubic force-deflection characteristics. The governing equations of motion for this system are given by

$$EI\ Y''''(x,t)+m\ddot{Y}(x,t)+c\dot{Y}(x,t)=0 \tag{8}$$

with boundary conditions

$$EI\,Y'''(0,t) = -k_1[Y(0,t) - u] - \alpha[Y(0,t) - u]^3;$$
$$EI\,Y'''(L,t) = k_2[Y(L,t) - v] + \alpha[Y(L,t) - v]^3;$$
$$Y''(0,t) = 0 \quad Y''(L,t) = 0;$$

and initial conditions as $Y(x, 0) = 0$, $\dot{Y}(x, 0) = 0$. Here, EI is flexural ridigity, m, the mass per unit length, c, the viscous damping coefficient, k_1 and k_2 are linear spring rates and α is nonlinear spring rate. It may be noted that the above governing equation of motion constitutes a nonlinear partial differential equation with randomly time-varying boundary conditions. The field equation here is linear but the nonlinearity enters through the boundary conditions. As the exact solution to this type of problems is currently not possible, one has to follow approximate analysis procedures or digital simulation strategies. We developed an approximate response analysis strategy which enables the determination of steady-state response statistics and to evaluate the acceptability of this approximation via Monte Carlo simulations. By applying the method of equivalent linearization, we replace the nonlinear springs by a pair of equivalent linear springs with spring rates β_1 and β_2. The field equation governing the behavior of the equivalent linear system is identical to eqn (1). However, the boundary conditions now get linearized and are modified to read

$$EI\,Y'''(0,t) = -\beta_1[Y(0,t) - u];$$
$$EI\,Y'''(L,t) = \beta_2[Y(L,t) - v];$$
$$Y''(0,t) = 0;$$
$$Y''(L,t) = 0.$$

To determine the equivalent linear spring rates β_1 and β_2, we demand that the average steady-state potential energy stored in the nonlinear system and the linearized system are the same. Consequently, the equivalent linear parameters β_1 and β_2 are obtained as

$$\beta_1 = k_1 + \frac{3}{2}\alpha\sigma_{z_1}^2;$$

$$\beta_2 = k_2 + \frac{3}{2}\alpha\sigma_{z_2}^2. \tag{10}$$

Here, $\sigma_{z_1}^2$ and $\sigma_{z_2}^2$ are variance of relative displacements $z_1(t) = [Y(0, t) - u(t)]$ and $z_2(t) = [Y(L, t) - v(t)]$ in the left and right springs, respectively. It must be noted that the equivalent spring rates β_1 and β_2 are functions of $\sigma_{z_1}^2$ and $\sigma_{z_2}^2$, which, in turn, depend upon β_1 and β_2. In other words, eqn (10) represents a pair of nonlinear equations for β_1 and β_2. To determine the equivalent parameters β_1 and β_2, we first obtain the PSD functions for the processes $z_1(t)$ and $z_2(t)$. This is done by carrying out a stationary response analysis of the equivalent linear system using dynamic stiffness matrix formulations. The accuracy of the approximation in linearization is assessed by using results from Monte Carlo simulations. Also, we consider the problem of response analysis when the input is partially specified. Specifically, we assume that the auto-PSD functions of the excitation components is known while the CPSD functions are not known. The problem of determining the critical and most favourable CPSD functions which, respectively, produce the highest and lowest steady-state response variance is considered.

5. Numerical results and conclusions

In the numerical work, it is assumed that external diameter $D_o = 0.1$ m, internal diameter $D_I = 0.072$ m, mass density $\rho = 2700$ kg/m^3, Young's modulus $E = 2.1e5$ N/m^2 damping constant C = 63.0 N-s/m^2, spring stiffness $k_1 = k_2 = 1.767e5$ N/m and length L = 8 m. The nonlinear spring rate α_1 and α_2 are taken to be in the range of 2.0E + 06 to 4.0E + 06.

It has been demonstrated that the response variance is significantly influenced by the choice of the cross-PSD functions. The earthquake ground motions are modeled as a vector of nonstationary gaussian random processes. The spatial variability of the ground motions is characterized in terms of cross-PSD functions. The method of equivalent linearization has been developed to analyze the response of a nonlinearly supported beam subjected to stationary random differential support motions. The response analysis is based on the use of beam dynamic stiffness matrices. An iterative method to evaluate the equivalent linear parameters has been developed. The performance of the approximations made is assessed by conducting digital simulation studies based on finite-element method. Satisfactory agreement between theoretical and simulated results has been demonstrated over a wide range of system parameters. The nature of cross-PSD functions which lead to the highest and lowest response variance has been established. It is shown that these optimal cross-PSD functions correspond neither to fully correlated motions nor to statistically independent motions. Instead, these spectra are dependent on system parameters, nature of information available on the input and functions of response variables chosen for optimization.

References

1. SARKAR, A. AND MANOHAR, C. S. Critical cross power spectral density functions and the highest response of multi-supported structures subjected to multi component earthquake excitations, *Earthquake Engng Struct. Dynamics*, 1996, **25**, 303–315.
2. SARKAR, A. AND MANOHAR, C. S. Critical seismic vector random excitations for multi-supported structures, *J. Sound Vibration*, 1998, **212**, 525–546.
3. MANOHAR, C. S. Methods of nonlinear random vibration analysis, *Sadhana*, 1995, **20**, 345–371.
4. MANOHAR, C. S. AND SARKAR, A. Critical earthquake input power spectral density function models for engineering structures, *Earthquake Engng Struct. Dynamics*, 1995, **24**, 1549–1566.

Thesis Abstract (M. Sc. (Engng))

Suppression of ACI in cellular mobile communications by G. Vijay Kumar

Research supervisor: Prof. A. P. Shivaprasad
Department: Electrical Communication Engineering

1. Introduction

Interference is the major limiting factor in the performance of cellular mobile communication systems. The two major types of system-generated interference in cellular mobile communica-

tion systems are co-channel interference (CCI) and adjacent channel interference (ACI). Co-channel interference is generally reduced by physically separating the co-channel cells by a minimum distance to provide sufficient isolation and ACI is reduced by proper designing of the transmitter and receiver filters[1–3] and frequency assignment plan such that no two adjacent frequencies are assigned to the same cell. Although channel filters in both the base station and the mobile unit significantly attenuate signal from adjacent channels, severe interference may occur under circumstances where the received signal level of an adjacent channel greatly exceeds that of the desired channel. This situation arises often in mobile cellular environments due to the distance difference between the mobile units and the base stations. Several DCA schemes[4–6] have been proposed to improve the quality and carried traffic in mobile cellular radio system. Most of these schemes assign channels to calls based on the constraint imposed by co-channel interference, and ignore the ACI constraints. Incorporating the ACI constraints results in increased call blocking probability. Therefore, it is necessary to develop a new scheme which has less call-blocking probability with the desired ACI constraints. Hence, in this work, we propose the channel swapping-based dynamic channel allocation (CS-DCA) scheme.

2. Channel swapping-based dynamic channel allocation (CS-DCA)

The scheme involves swapping the assigned channels from the interfering cells to assign a channel for a call request which is about to fail due to ACI constraints. This scheme can be applied to any DCA scheme for more efficient frequency utilization. Hence, the scheme is called channel swapping-based dynamic channel allocation (CS-DCA).

Let us consider a cell c. Suppose $AVL(c)$ is set of interfering cells of cell c, $ASS(c)$ is a set of assigned channels in cell c, $INTF(c)$ is a set of interfering cells of cell c, f_1 is minimum channel separation between simultaneous calls in a cell, and f_2 is minimum channel separation between simultaneous calls in a cell and its adjacent neighbours. Then to swap the channels $ch1 \in ASS(c)$, $ch2 \in ASS(k)$, where $k \in INTF(c)$ to assign the channel $ch \in AVL(c)$ in cell c,

(i) Channel $ch1$ should not have been assigned in any of the interfering cells of cell k, except in cell c. This is represented by swap constraint

$$S_{ck}(ch1) = \begin{cases} 0 & \text{if } ch1 \notin \{ASS(j)\} \text{ where } j \in INTF(k),\ j \neq c \\ 1 & \text{otherwise} \end{cases} \tag{1}$$

(ii) Similarly, Channel $ch2$ should not have been assigned in any of the interfering cells of cell c, except in cell k, which is represented by

$$S_{kc}(ch2) = \begin{cases} 0 & \text{if } ch2 \notin \{ASS(j)\} \text{ where } j \in INTF(c),\ j \neq k \\ 1 & \text{otherwise} \end{cases} \tag{2}$$

(iii) Channel $ch1$ should satisfy the required ACI constraints in cell k. It is represented by

$$d_{ck1}(ch1) \geq 0,\ d_{ck2}(ch1) \geq 0 \tag{3}$$

where

$$d_{ck1}(ch1) = \min\{|ch1 - i| : i \in ASS(k), i \neq ch2\} - f_1;$$
$$d_{ck2}(ch1) = \min\{|ch1 - j| : j \in ASS(k1), \text{ where } k1 \in INTF(k), k1 \neq c\} - f_2.$$

(iv) Channel $ch2$ should satisfy the required ACI constraints in cell c, and channel $ch2$ should also satisfy the required channel separation with channel ch in cell c. For this,

$$d_{kc1}(ch2) \geq 0,\ d_{kc2}(ch2) \geq 0, \text{ and } d_{kc}(ch2) \geq 0 \tag{4}$$

where

$$d_{kc1}(ch2) = \min\{|ch2 - i| : i \in ASS(c), i \neq ch1\} - f_1$$
$$d_{kc2}(ch2) = \min\{|ch2 - j| : j \in ASS(k1), \text{ where } k1 \in INTF(c), k1 \neq k\} - f_2$$
$$d_{kc}(ch2) = |ch2 - ch| - f_1$$

and from (iii) and (iv), the frequency separation constraint (FSC) is represented by

$$FSC_{ck}(ch, ch1, ch2) = \begin{cases} 0 \text{ if } d_{ck1} \geq 0, d_{ck2} \geq 0, d_{kc1} \geq 0, \\ \quad d_{kc2} \geq 0, \text{ and } d_{kc} \geq 0 \\ 1 \text{ otherwise.} \end{cases} \tag{5}$$

Then, the overall cost function C_{ck} for the channel swapping is expressed as

$$C_{ck}(ch, ch1, ch2) = S_{ck}(ch1) + S_{kc}(ch2) + FSC_{ck}(ch, ch1, ch2). \tag{6}$$

So, if the cost function $C_{ck}(ch, ch1, ch2) = 0$, channels $ch1$, $ch2$ are swappable such that channel ch can be assigned in cell c.

3. Vehicle location in cellular mobile communication system

In the above section, the frequency separation constraints required for suppression of ACI are calculated with the worst-case assumptions (i.e. far-end mobile is at the boundary of the cell and near-end mobile is 50 m away from the base station). To further improve the system performance, the mobile location has to be considered while calculating the required ACI constraints. For this, we propose a scheme, least square estimation (LSE), to estimate the location of the mobile in cellular communication system. In contrast to the methods[7, 8] our scheme uses signal strength received from the mobile at three base stations, for locating the mobile and the LSE to reduce error. Then a cell is divided into three concentric circular regions (of radii 500, 1000 and 1500 m) and assuming that the mobile could be in any one of the regions, a frequency separation matrix (F, shown below) is prepared which satisfies the ACI constraints.

$$\mathrm{F} = \begin{pmatrix} f_{11} & f_{12} & f_{13} \\ f_{21} & f_{22} & f_{23} \\ f_{31} & f_{32} & f_{33} \end{pmatrix} = \begin{pmatrix} 3 & 4 & 5 \\ 4 & 2 & 2 \\ 5 & 2 & 2 \end{pmatrix}$$

4. Channel allocation using frequency separation matrix

We consider the DCA95 scheme proposed,[9] and obtain a cost function for assigning a channel with ACI constraints using frequency separation matrix. For simplicity, we neglect the adjacent channel interference from the neighbouring cells. The scheme involves,

- *Assign the channel that is available in the smallest number of interfering cells.*

  The allocation cost contribution for the channel $ch \in AVL(c)$ for the above statement can be expressed as

$$C1_c(ch) = \sum_k \{A_k(ch)\} \text{ where } k \in INTF(c) \text{ and } A_k(ch) \text{ is given by} \tag{7}$$

$$A_k(ch) = \begin{cases} 1 & \text{if } ch \in AVL(k) \\ 0 & \text{otherwise.} \end{cases}$$

  To assign an optimal channel $ch \in AVL(c)$ in cell c, cost function for each channel $ch \in AVL(c)$ is calculated and the channel, ch, which gives minimum $C1_c(ch)$ is assigned.

- *Assign the channel that is available in the smallest number of interfering cells and also satisfy the required frequency separation.*

$$d_1(ch) = \min\{|ch - i| : \quad i \in ASS_1(c)\} - F[r][1]$$
$$d_2(ch) = \min\{|ch - i| : \quad i \in ASS_2(c)\} - F[r][2]$$
$$d_3(ch) = \min\{|ch - i| : \quad i \in ASS_3(c)\} - F[r][3]$$

  where $ASS_1(c)$ is the set of channels assigned in region 1 of cell c

  $ASS_2(c)$ is the set of channels assigned in region 2 of cell c

  $ASS_3(c)$ is the set of channels assigned in region 3 of cell c

  $F[r][1]$, $F[r][2]$ and $F[r][3]$ are the 1st, 2nd and 3rd elements of the rth row of the matrix $\mathbb{F}$, where r is the region in which the call is arrived.

The allocation cost contribution for the channel $ch \in AVL(c)$ can be expressed as

$$C2_c(ch) = \begin{cases} 0 & d_1(ch) \geq 0 \ \&\& \ d_2(ch) \geq 0 \ \&\& \ d_3(ch) \geq 0 \\ 1 & \text{otherwise.} \end{cases} \tag{8}$$

From eqns (7) and (8), the channel allocation cost function C_c, incorporating the ACI constraints can be expressed as

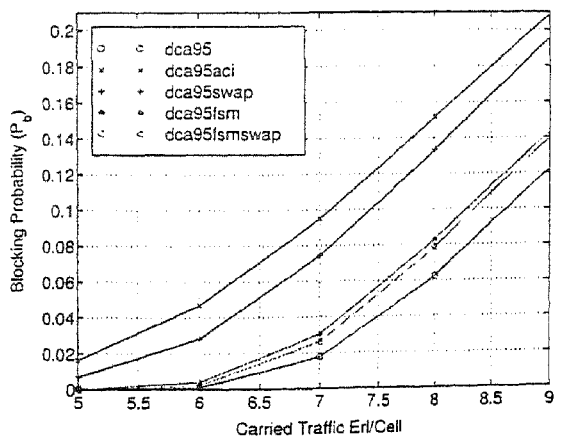

FIG. 1. Blocking probability (P_b) vs carried traffic (Erl/cell) for scheme DCA-95.

$$C_c(ch) = C1_c(ch) * C2_c(ch). \quad (9)$$

To assign an optimal channel $ch \in AVL(c)$ in cell c with ACI constraints, overall cost function for each channel $ch \in AVL(c)$ is calculated and the channel, ch, which gives $C_c(ch) = 0$ is assigned. Otherwise, optimal channel is not available and the call is blocked.

5. Conclusion

Performance of the channel swapping-based dynamic channel allocation (CS-DCA) using frequency separation matrix (FSM) in terms of call-blocking probability (P_b) at different carried traffics has been studied using computer simulation. It is observed that the proposed scheme reduces significantly the call-blocking probability (Fig. 1), while meeting the desired ACI constraints.

References

1. KINOSHITA, N. — Method of rejecting adjacent channel interference using an adaptive equalizer, *Electron. Commun.*, Part 1, 1989, **72**(11), 1–10.
2. UESUGI, M., HONMA, K. AND TSUBAKI, K. — Adaptive equalization in TDMA digital mobile radio, *Proc. Globecom'89*, Vol. 1, 1989, pp. 95–101.
3. UESUGI, M., FUTAGI, S. AND HOMM, K. — Interference cancellation method using DFE, *IEEE Veh. Technol. Conf.*, 1996, pp. 1190–1194.
4. CHAUNG, J. — Autonomous adaptive frequency assignment for TDMA portable radio systems, *IEEE Trans.*, 1991, **VT-40**, 627–635.
5. CHENG, M. AND CHUANG, J. — Distributed measurement-based quasi-fixed frequency assignment for personal communications, *Proc. IEEEICC'95*, Seattle, 1995, pp. 433–437.
6. OH, S. H. — Prioritized channel assignment in a cellular radio network, *IEEE Trans.*, 1992, **C-40**, 1259–1269.
7. OTT, G. D. — Vehicle location in cellular mobile radio systems, *IEEE Trans.*, 1977, **VT-26**, 43–46.
8. SONG, H.-L. — Automatic vehicle location in cellular communication systems, *IEEE Trans.*, 1994, **VT-43**, 902–908.
9. DEL RE, E. AND FANTACCI, R. — Handover and dynamic channel allocation techniques in mobile cellular networks, *IEEE Trans.*, 1995, **VT-44**, 229–237.

Thesis Abstract (M. Sc. (Engng))
Formation of cream in emulsions by A. V. Ganesh
Research supervisor: Dr Sanjeev Kumar Gupta
Department: Chemical Engineering

1. Introduction

Emulsions are liquid–liquid dispersions stabilized by surface-active agents called surfactants. The dispersed phase drops are typically of the order of 10 μm in size. Emulsions have a wide

range of applications from medicinal and food products to explosives. Emulsions, in their capacity to retain the two phases in the original form, have a peculiar exposition of characteristics of both phases.

These emulsions often warrant storage. Even though emulsions are stabilized by surfactants, they have a finite shelf-life. Naturally, longer shelf-life is always desirable. The shelf-life can be improved only when the mechanisms dictating the breakdown process of emulsion are understood. The breakdown can be predicted only after understanding all the subprocesses involved. The present work is an attempt to understand one of the subprocesses of the breakdown of emulsion, namely, formation of cream.

2. Objective

Typically, when a freshly prepared uniform (polydisperse) emulsion is left undisturbed, the dispersed drops being lighter than the continuous phase migrate due to buoyancy and collect (and pack) at the top of the container to form cream. The present work aims at prediction of the spatial and temporal drop size distribution in the cream.

3. Model development

Consider a freshly prepared emulsion stored in a container in which the drops are creaming. The governing population balance equation has been derived for the creaming process based on number balance. The creaming dynamics which governs the formation of cream is characterised by the hindered creaming velocity of drops. The hindered creaming velocity, required in the convective term of the balance, was estimated by extending the experimental correlation for the creaming velocity of drops in monodispersed emulsion[1] to a multidisperse system.[2] The final set of the model equation is very complicated, hence an alternative approach has been adapted to solve them.

The continuous population was discretized into fine bins and population in each bin was represented through a representative volume. The governing integro partial differential balance equation was then simplified to balance the equation for population of drops in every bin.

Many modes of creaming are possible based on the Kynch's theory[3] for sedimentation in monodisperse suspensions. Simple settling is the simplest mode which normally exists only for very dilute dispersions. In this mode of settling, the information flows in only one direction and discontinuities separate zones (layers) having different compositions of drops. The governing differential equations thus reduce to simultaneous nonlinear algebraic equations. Typically, if layer 0 represents cream containing all the sizes, the layer just below the cream, called layer 1, contains moving drops of all the sizes. The layer below layer 1, layer 2, contains drops of all the sizes except the largest drops which have already creamed off into layer 1. In this manner, n layers can be tracked and below it will be the clear fluid.

The governing equations can be solved to capture the complete creaming dynamics and the spatial and temporal drop size distribution in the cream on knowing the initial distribution and the experimental parameter, the maximum total volume fraction in cream.

4. Solution methodology

4.1. *Simple creaming*

Standard methods like the Newton method and multidimensional bisection were attempted to solve the algebraic equations. As there were sharp continuities in the function to be solved, the Newton method failed. The multidimensional bisection turned out to be computationally very expensive. As none of the standard methods could be used, the nonlinear algebraic equations were then simplified using suitable substitutions into a single equation in terms of the total volume fraction in a particular layer.

4.2. *Complex creaming: Generalized equations*

The generalized model equations were solved to capture all the other modes of creaming. Solution of generalized simultaneous nonlinear hyperbolic partial differential equations was attempted using analytical, semi-analytical and numerical techniques.

It was found that the analytical techniques failed as the family of the characteristics could not be decoupled purely analytically due to the nonlinearity of the equations. A semi-analytical method was attempted by numerically estimating the transformation operator at each time and at all physical locations (grid points). The reverse transformation was difficult as the characteristics belonging to a particular family could not be tracked. It was also found that the second-order Lax–Wendroff[4] finite difference scheme could not even predict the dynamics of the creaming process which dictates the packing of drops in the cream. The third- and fourth-order schemes[4] were found to predict both the dynamics and the drop size distribution in the cream. These schemes are dispersive in nature and also become numerically unstable at (i) low volume fractions, and (ii) when discontinuities propagating in the opposite directions meet or after sudden introduction of time discontinuity.

5. Experiments

A 40 mm diameter cylindrical column of 1000 mm length was fabricated with a slit of 2×200 mm along the wall of the column for sampling. The slit was sealed with a self-curing sealant. Experiments were performed using a nonsurface active dispersed phase paraffin oil and glycerol–water mixture as continuous with sodium lauryl sulphate as surfactant to measure the drop size distribution in cream as a function of height and time. Emulsion was prepared in a mixer with impeller of Rushton type (55 mm diameter with 6 blades each of 10×20 mm). A closed type baffle was used to ensure minimal air trap. The emulsion was prepared in the vessel at known speed for about 120 min and was then immediately transferred into the column and was allowed to cream. Samples were withdrawn from the slit at various time steps at various heights while the cream formation was continuing. The height of the cream and the serum layer (liquid at the bottom with no oil droplets in it) formed were also monitored. The creaming was assumed complete when the height of the cream remained unchanged for a long time.

A few drops withdrawn from the sample were placed on a slide and viewed under microscope under different magnifications. Pictures were then taken using a video grabber. The diameter of the bubbles in the grabbed picture was measured using Sigma Scanpro Image Analy-

sis software (Jandel). The drop size distribution was then estimated by making suitable transformation of the measured raw diameter data.

6. Results and discussion

6.1. *Simple creaming mode*

The equations showed that the velocity of the smaller drops can become negative under certain conditions. Another interesting feature was that when the large drops cream off (because they move faster), the smaller drops left behind get concentrated. This could lead to a technique to concentrate particles without requiring them to settle completely and then resuspending them. These features are explained in detail for creaming of bidisperse emulsion. The nonlinear algebraic equations were solved for the initial drop size distribution obtained from the experiments. The model qualitatively predicts the experimental data, but overpredicts the creaming velocity and therefore predicts creaming to be faster than that observed experimentally.

6.2. *Complex-creaming mode*

The predictions were verified with the experimental data[5] reported in the literature for volume fraction profile at various times for a mono- and tridispersed emulsion. The model qualitatively predicts the volume fraction profiles. Further, it was found that the predictions could reflect two of the complex modes of creaming suggested by Kynch[3] theory of sedimentation. The model was also able to track the second kind of discontinuity that is likely to be operational at high volume fractions.

References

1. RICHARDSON, J. F. AND ZAKI, W. N. — Sedimentation and fluidisation: Part I, *Trans. Instn Chem. Engrs*, 1954, **32**, 35.
2. MIRZA, S. AND RICHARDSON, J. F. — Sedimentation of suspensions of particles of two or more sizes, *Chem. Engng Sci.*, 1979, **34**, 447.
3. KYNCH, G. J. — A theory of sedimentation, *Trans. Faraday Soc.*, 1952, **48**, 166.
4. LAPIDUS, L. AND PINDER, G. F. — *Numerical solution of partial differential equations in science and engineering*, Wiley, 1982.
5. WEDLOCK, D. J., FABRIS, I. J. AND GRIMSEY, J. — Sedimentation in polydisperse particulate suspensions, *Colloids Surf.*, 1990, **43**, 67.

Thesis Abstract (M. Sc. (Engng))

Graph algorithms for loss minimization through feeder reconfiguration by S. Kartik Krishnan

Research supervisor: Prof. P. S. Nagendra Rao
Department: Electrical Engineering

1. Introduction

Utilities are introducing distribution automation (DA) to remotely monitor, coordinate and operate distribution network components in real time. One of the DA functions at the customer

service level is feeder reconfiguration. Feeder reconfiguration entails altering the topological structure of the distribution feeders, by remotely controlling the on/off status of these tie and sectionalizing under both normal and abnormal operating conditions. The benefits of feeder reconfiguration include restoring power to outaged portions of a feeder in a timely manner, relieving of overloads on feeders by shifting load in real time to adjacent feeders and reducing resistive line losses.

This work addresses methods of determining the configuration with reduced power losses. This is a combinatorial optimization problem. A combinatorial search of all switching operations is not feasible as the problem is to be solved in real time. Also, complicating the problem are the nonlinear nature of the objective function and various constraints such as radiality, voltage profile, current capacity of components, etc.

2. Existing methods of solution

In recent times, considerable research has been conducted in the area of loss minimization. A good overview of these schemes is available in Sarfi *et al.*[1] These techniques can be classified into the following categories.

1. *Heuristic methods employing empirical formulae*: These methods start with an initial configuration and attempt to find the optimum switching operations, either one pair at a time or more complex switching strategies such as a series of branch exchanges. These methods use heuristic rules and/or empirical formulae to assess the loss reduction with each switching operation. However, these methods only seek local optimal solutions.
2. *Techniques based on mathematical programming*: The various techniques in this set formulate the problem, using ideas from mathematical programming such as nonlinear, linear and integer programming, branch and bound techniques, etc. Although mathematically rigorous, these schemes are too time-consuming and hence are not viable schemes, especially for large test systems.
3. *AI-based methods*: Here techniques like simulated annealing (SA), Tabu search, genetic algorithms (GA), artificial neural networks (ANNs) and expert systems based on heuristic rules have been used. However, these methods become cumbersome for systems of realistic sizes with the added system constraints. Techniques such as SA, Tabu search and GA are randomized schemes which typically require a number of reruns before they converge to a reasonable solution. Moreover, ANNs and expert systems are only as accurate as the training examples provided.
4. *Methods based on successive load flow solutions*: There have been two alternative approaches to solution.
   (a) The first approach is due to Shirmohammadi and Hong.[2] Here the final radial configuration is obtained using an iterative technique, the initial stage of which consists of closing all the switchgears and solving the meshed network thus created. The flows in the respective lines are obtained and the switchable branch with the lowest flow is opened, thus creating a network with fewer meshes. The procedure is repeated until there are no further meshes in the system.

(b) The second approach due to Goswami and Basu[3] begins with the prevailing network configuration. Here the closure of a switch during each iteration is complemented by the opening of another, thereby ensuring that the system is radial at the start and at the end of each iteration. The method begins with one of the initially open tie switches and terminates when all the tie switches have been considered.

These methods based on successive network solutions represent the most promising schemes of solution so far. A network flow solution has to accompany every opening of a mesh. The network solutions however represent a considerable computational burden and are infeasible when the number of meshes to be broken is large.

3. The proposed approach

Our work begins with the investigation whether it is possible to solve this problem in one iteration alone. We begin with the meshed configuration as in the first approach to take global view of the problem as a whole. We establish that it is sufficient to perform only one load flow solution on the initial meshed configuration and utilize these results alone to choose a set of switches to be opened. This is done with a view to perturb the network in the least possible from the initial meshed configuration which corresponds to the minimum loss network configuration. In view of this, when the distribution network is represented by means of a graph, with the substation transformers and the customer loads representing the nodes of the graph and the feeder sections representing weighted edges, the idea of removing a set of line sections with low current is topologically equivalent to removing a set of edges in this graph with small weight.

We investigate three graph theoretic schemes for this purpose.

3.1. *Algorithms based on graph partitioning*

Graph partitioning attempts to place heavy weight edges in the partition sub-blocks, whereas a set of low weight edges form the cutset, i.e. the set of edges cut. A scheme regarding the use of graph partitioning has already been presented in the literature by Sarfi *et al.*[4] This scheme has limitations regarding the choice of the initial configuration and choice of weights. We propose an improved scheme which utilizes Barnes' algorithm.[5] However, Barnes algorithm requires that the partition sizes be specified *a priori*. This difficulty is overcome by spectral graph partitioning[6] which computes an edge separator from eigenvector components of the Laplacian matrix of the graph.

Owing to the computation involved in the Laplacian eigenvector, especially in the larger test cases, we propose a number of methods to compress the graph. The compression techniques discussed include recursively removing the degree one nodes in the graph, removing the articulation points[7] in the graph and compressing the graph via a maximum weight matching.[8]

We also propose a scheme which utilizes the spectral information, together with the *orientation* of the currents in the edges to compute a partition.

3.2. *Algorithms based on maximum spanning tree (MST)*

An MST is a spanning tree of a graph, the sum of whose edge weights is maximum.[7,8] This scheme can be applied to both the single and multiple transformer test cases. We present two alternate approaches[9] to constructing an MST. The primal approaches construct the MST edge by edge, including appropriate heavy weight edges. The dual approaches begin with the entire graph and construct an MST by removing appropriate low weight edges. The latter approach is especially useful in test examples, when the number of meshes is small.

3.3. *Algorithms based on optimum branchings*

A branching of a directed graph is a subgraph which has no cycles and where the number of edges incident and directed towards each node is at the most one. An optimum branching is a branching whose total edge weight is maximum.[10] This scheme exploits the directed acyclic (dag) nature of the distribution graphs. This property ensures that we can do away with the extra computation required for checking loops in the spanning tree class of algorithms.

The proposed algorithms have been thoroughly tested by considering a number of test systems (sizes varying from 11 to 1158 nodes) and comparing their performance with those of the existing algorithms.

A critical assessment of the three schemes, i.e. their relative efficiency, salient features and shortcomings, is made with those presented in the literature.

4. Conclusions

It is felt that a beginning has been made here to provide a range of potentially very efficient algorithms for the loss minimization problem. Both single and multiple transformer cases have been considered. It is envisaged that the algorithms developed here would find their place, being very fast and efficient, in the implementation of feeder reconfiguration algorithms in distribution automation.

References

1. SARFI, R. J., SALAMA, M. M. A. AND CHIKANI, A. Y. — A survey of the state of the art in distribution system reconfiguration for system loss reduction, *Elect. Power Energy Systems*, 1994, **31**, 61–70.
2. SHIRMOHAMMADI, D. AND HONG, H. W. — Reconfiguration of electric distribution networks for resistive line loss reduction, *IEEE Trans.*, 1989, **PD-4**, 1492–1498.
3. GOSWAMI, S. K. AND BASU, S. K. — A new algorithm for the reconfiguration of distribution feeders for loss minimization, *IEEE Trans.*, 1992, **PD-7**, 1484–1491.
4. SARFI, R. J., SALAMA, M. M. A. AND CHIKANI, A. Y. — Distribution system reconfiguration for loss reduction: An algorithm based on network partitioning theory, *IEEE Trans.*, 1996, **PS-11**, 504–510.
5. BARNES, E. R. — An algorithm for partitioning the nodes of the graph, *SIAM J. Algebraic Discrete Methods*, 1982, **3**, 541–550.
6. POTHEN, A., SIMON, H. D. AND LIOU, K. P. — Partitioning sparse matrices with eigenvectors of graphs, *SIAM J. Matrix Analysis Applic.*, 1980, **11**, 430–452.

7. AHO, A. V., HOPCROFT, J. E. AND ULLMAN, J. D. *The design and analysis of computer algorithms*, Addison–Wesley, 1974.

8. PAPADIMITRIOU, C. H. AND STEIGLITZ, K. *Combinatorial optimization, algorithms and complexity*, Prentice-Hall, 1982.

9. TARJAN, R. E. *Data structures and network algorithms*. Society for Industrial and Applied Mathematics, Philadelphia, Pennsylvania, 1983.

10. THULASIRAMAN, K. AND SWAMY, M. N. S. *Graphs: Theory and algorithms*, Wiley, 1992.

Thesis Abstract (M. Sc. (Engng))

Effects of data pre-processing on transfer function and coherence function computed during impulse tests on transformers by V. Jithendra

Research supervisor: Dr L. Satish

Department: High Voltage Engineering

1. Introduction

Impulse test is considered as an efficient quality control procedure applied to power transformer, which can reveal defects in insulation structures caused during manufacture or thereafter while in service.[1, 2] During this test, a transformer is subjected to a special sequence of full and chopped impulses, at full and reduced test levels as per existing standards. Then, the assessment is based on interpretation of test data and for this many methods like voltage oscillogram method, neutral current method, transferred surge current method, etc. have been in use. However, these conventional methods have some limitations such as dependence of output response on input excitation, thick trace of oscillograms, etc., which make interpretation rather difficult, if not impossible.

A major breakthrough in data interpretation was achieved with the introduction of digital techniques in high-voltage impulse testing and measurements. The main advantage of this was the availability of test data in digital form, paving way for the use of signal processing principles, which led to the development of transfer function (TF)[1, 2] and coherence function (CF)[3] methods. However, the underlying A/D conversion process causes signals to be non-ideal. Other factors which cause the acquired signals to be non-ideal are noise, interference, sampling errors, dynamic nonlinearities within the digitizers, etc. If this raw data are directly used to compute TF and CF, it will result in excessive noise and thereby make unambiguous interpretation rather difficult. Thus, it necessitates pre-processing of data prior to performing any other computation.

Recognising this fact, many commercial softwares (that nowadays accompany impulse test systems) adopt a variety of filtering, windowing, weighting, and threshold procedures, with the ultimate goal of producing smooth-looking TF and CF. However, some of these pre-processing operations can introduce large deviations in the computed TF and CF. To further complicate matters, most softwares are not transparent about operations they perform.[4] Therefore, it is all the more necessary to analyze the influence of data pre-processing operations on TF and CF. These were the main motivating factors to initiate this research work. This work focuses attention on the following issues:

- Investigation of effects due to different factors and pre-processing operations on TF and CF.
- Propose ways of overcoming some of these effects.
- Deduce a procedure for correct estimation of TF and CF.

2. Data processing issues in TF

Post-digital era in high-voltage impulse testing achieved a significant landmark with the introduction of the TF method. The underlying principle of this method assumes transformer as a linear time invariant (LTI) system. The TF of a transformer is defined as the ratio of the Fourier transform of the neutral current to the Fourier transform of the impulse voltage. Mathematically, it is given by,

$$TF = H\left(e^{j\omega}\right) = \frac{Y\left(e^{j\omega}\right)}{X\left(e^{j\omega}\right)}, \tag{1}$$

where $Y(e^{j\omega})$, $X(e^{j\omega})$ and $H(e^{j\omega})$ are, respectively, the frequency domain representations of the neutral current, $y[n]$, impulse voltage, $x[n]$ and impulse response, $h[n]$. Even though the above equation appears to be a straightforward mathematical operation, it must be emphasized that it is defined and valid only when both $x[n]$ and $y[n]$ are ideal. But, in practice all acquired signals are non-ideal. This non-ideal nature of the signal manifests as high-frequency noise, whose direct consequence is to alter the shape of the TF. Therefore, TF is a sensitive tool and is influenced by different factors and signal processing operations.[4]

In the first part of the thesis, various factors and pre-processing operations like quantization, record length, initial delay, windowing, Nicolson weighting, filtering, etc. which can have influence on the computed TF are identified. The contributions of each of these operations are described by conducting simulation studies with analytical data (these data allowed computation of an exact TF which was used as a benchmark for comparisons). From this study, it can be concluded that a direct comparison of TFs computed with full- and chopped-wave is always not possible. The presence of the chopped-wave voltage spectrum will be beneficial for making such a comparison more meaningful. The initial delay and chopping action have almost similar effects on TF. Both cause periodic oscillations with a period equal to the inverse of initial delay or chopping time in the computed TF. The initial delay in signals has significant influence on the computed TF when record lengths are less than 4 K. Also, most often the signals recorded are finite in duration due to memory limitations, which cause truncation of the signals. This results in leakage when the frequency spectrum is computed. Different window functions were discussed to reduce this leakage effects. The symmetrical window functions are not suitable for this application. Nonsymmetrical windows like exponential window, modified Hanning window and Nicolson weighting yielded comparatively better results. However, Nicolson weighting yields good results, when recorded signals have high truncation values at both ends or one of the ends. Suitable low-pass filtering effectively reduces the high frequency noise in the calculated TF. All these results are validated with model data (4 K length, obtained from experiments carried out by using a repetitive surge generator and a model transformer coil) and another from an actual test on a transformer, J-data (12 K length) circulated by

CIGRE, Working Group 33-03, Task Force 1.1. Thus, it was demonstrated that almost all data pre-processing operations have some influence on the shape of TF. Therefore, it is proposed that all TF data must invariably include information on the pre-processing performed and thereby aid in better evaluation of the impulse test data.

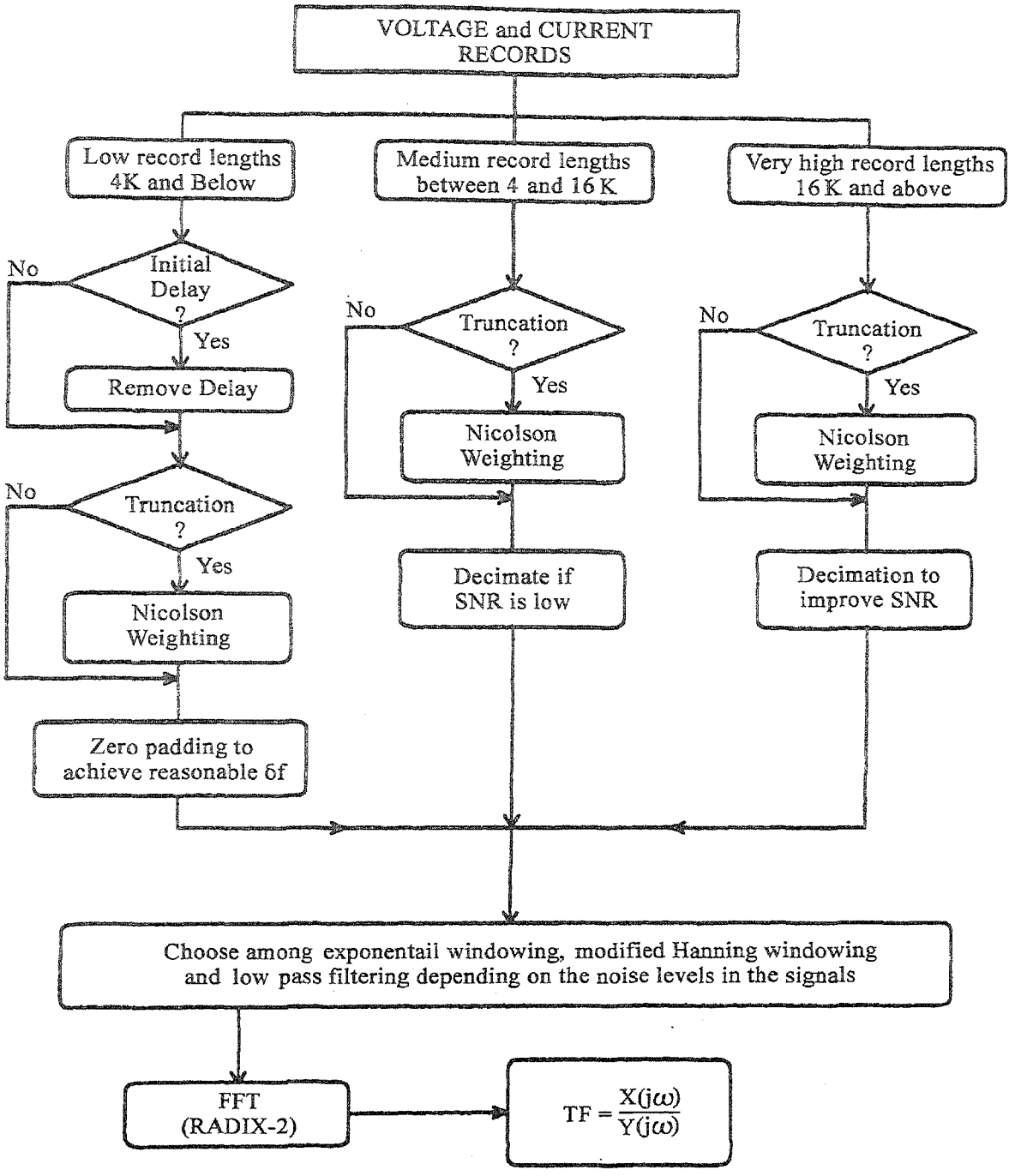

FIG. 1. Decision-tree for computation of transfer function.

3. Issues in CF estimation

A new fault diagnosis tool emerging in the field of high-voltage impulse testing is the coherence function (CF). This function provides frequency information at which signals have been affected by noise or interference. Though it has proved to be a good tool to check the presence of interference effects on records and also for fault diagnosis, it must be emphasized that it has not made its existence in real world because of the following limitations.

- Results in ambiguity when full- and chopped-wave data are pooled.
- Influenced by many factors and pre-processing operations.

The interaction between the various pre-processing operations and computed CF is also discussed, first with the analytical data followed by the two sets of practical data. In general, the effects are more or less similar to those observed in the case of TF. It is clearly shown that pooling of full- and chopped-wave data while computing coherence results in low coherence values. However, these low values should not be interpreted as due to fault or interference. It was observed that coherence is definitely a sensitive tool, and therefore, extra caution must be exercised with the data pre-processing.

4. Decision-trees to compute TF and CF

Based on the effects of various pre-processing operations on TF, a decision-tree is developed, which indicates what processing should be done on signals of different record lengths to achieve a good estimate of TF. Figure 1 shows the decision-tree for computation of TF. The assumptions made for voltage and current records while developing this tree are as follows:

- Sampling interval, T_s: 20–50 ns.
- Desirable frequency resolution in TF, δf: 5–10 kHz
- Record duration, T: 100–500 μs.

First, truncation, if any, must be removed and then radix-2 FFT is used to compute frequency spectrum of the signal. If record lengths that are not a power of 2 are encountered, then the corresponding records are padded with zeros. After this padding, if any high-frequency noise is present in the signal, it can be eliminated by using either exponential window, modified Hanning window or low-pass filtering depending upon the circumstances. Nevertheless, the pre-processing procedure adopted should be clearly made known such that meaningful comparison of TFs is possible.

A standard impulse test data is considered, i.e. two full-wave impulses (reduced and full levels), two chopped-waves and two full waves (full and reduced levels) to develop the decision-tree for CF. The decision-tree for CF is shown in Fig. 2. It involves the following steps:

- Compute coherence for the first set of full waves after removing truncation, if present.
- Compute coherence of the two chopped-wave records.
- Compute coherence for the second set of full-wave records, obtained after chopped-wave tests.

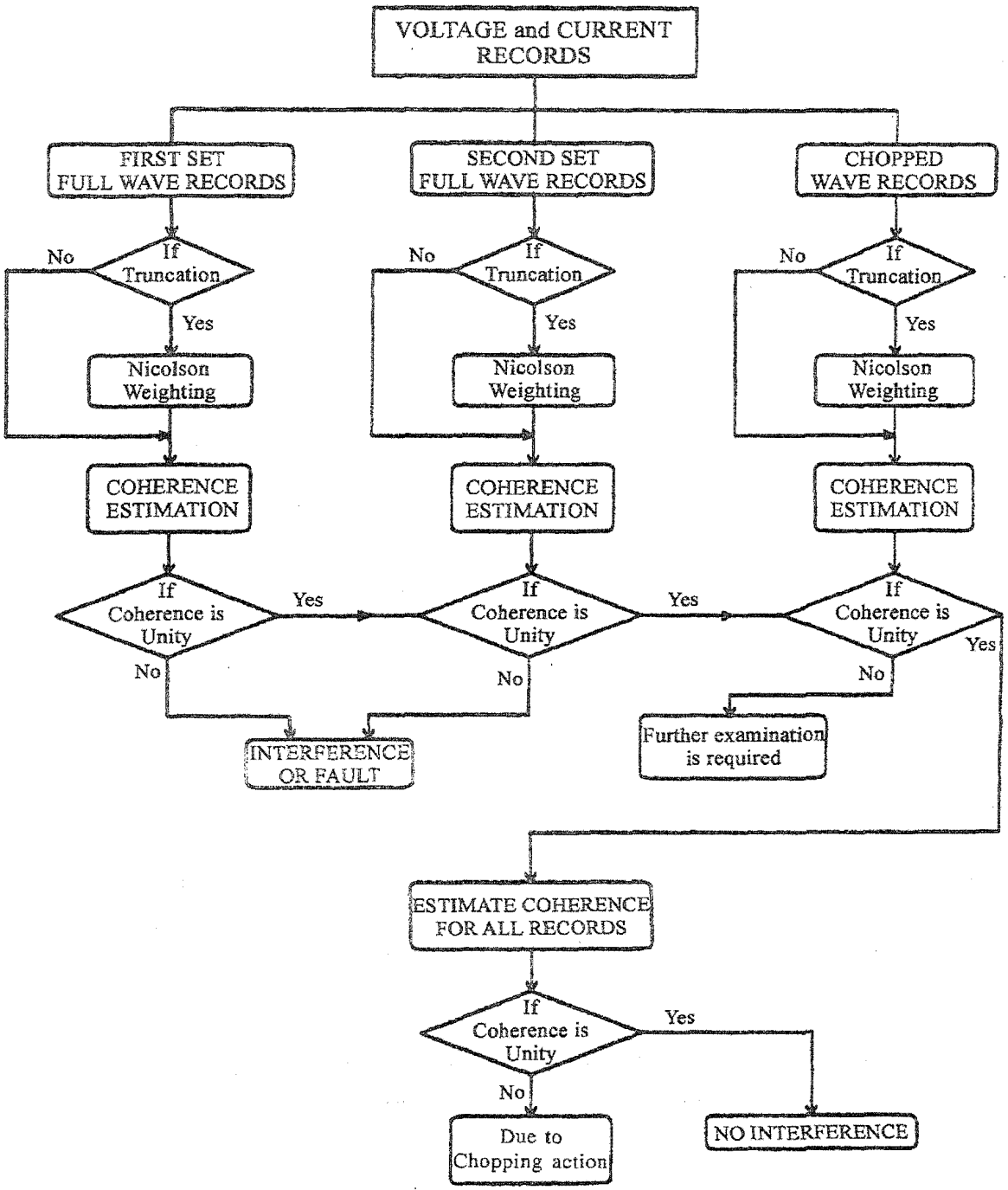

FIG. 2. Decision-tree for computation and interpretation of coherence function.

- If the coherence computed from the first set of full waves is less than unity in a limited frequency range, then there may be interference or fault. Coherence computed from the second set of full waves is also interpreted in the same manner.

- If both these full-wave coherences are unity then coherence computed with chopped-waves is checked. If the coherence is less than unity and periodic dips are observed, then it is due to the differences in chopping times. If this is also unity then coherence is computed by pooling all the impulse test data.
- If the coherence computed for all the data sets is unity in a limited frequency range, then there is no interference or fault. Otherwise, coherence is affected by the chopping action.

5. Conclusions

The computation of TF and CF from raw impulse test data poses mathematical difficulties and ambiguities with interpretation. This necessitates pre-processing the data prior to any other computation. However, some of the pre-processing operations can have significant influence on the TF and CF. The effects of various factors and pre-processing operations such as initial delay, windowing, Nicolson weighting, chopping, quantization, finite record length, etc. on TF and CF are investigated with analytical and practical data. Based on all these results and observations, a decision-tree was developed to compute TF for different record lengths. A similar tree was deduced for achieving a systematic computation and improved interpretation of the CF.

References

1. MALEWSKI, R. *et al.* — Five years of monitoring the impulse test of power transformers with digital recorders and the transfer function method, *CIGRE*, 1992, pp. 12–201.
2. LEIBFRIED, T. AND FESER, K. — Insulation diagnostics of power transformers by means of the transfer function method, *8th Int. Symp. on High Voltage Engineering*, Yokohama, Japan, Aug. 23–27, 1993, paper 65.02.
3. CLAUDI, A. *et al.* — Checking electromagnetic compatibility of a HV impulse measuring circuit with coherence functions, *Haefely Trench Symp.*, 1995.
4. GURURAJ, B. I. AND SATISH, L. — Some thoughts on transfer function and coherence in lightning impulse testing of transformers, *CIGRE 33-98 (WG 03)*, 32 IWD, Joensuu, Finland, 1998.

Thesis Abstract (M. Sc.(Engng))

Optical tomographic microscope for quantitative imaging of phase objects by N. Jayshree

Research supervisor: Prof. R. M. Vasu

Department: Instrumentation

1. Introduction

Optical tomography is about the reconstruction of object refractive index distribution $n(x, y, z)$ from the optical path delay (opd) measurements $\int_n(x, y, z)ds$. A tomographic microscope[1] for the cross-sectional imaging of fibers and optical waveguides which are non-absorbing (i.e. their refractive index distributions are real) is developed. The following problems are

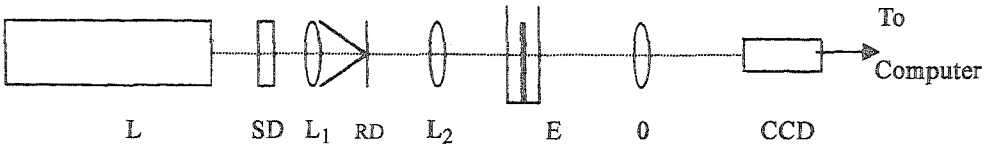

FIG. 1. The laboratory model of the tomographic microscope. The imaging (O) is a 3× objective.

addressed: (i) Wavefront estimation through a robust and easily implemented method and (ii) Reconstruction of the phase delay data with refraction correction for accurate quantitative estimate of refractive index distributions which define the object. We report efficient methods[2] to solve the intensity transport equation (TIE)[3] given by

$$k * \partial_z I = -\nabla \cdot (I \nabla \phi) \tag{1}$$

which relates the transverse-plane phase (Φ) to the rate of change of intensity $\partial I/\partial z$, along the axis to obtain $\Phi(x, y)$ from $\partial I/\partial z$. Here k is the propagation vector. A first estimate of the refractive index distribution of the object is obtained by using the convolution back projection (CBP)[4] algorithm on the measured phase delay data under the assumption of straight line propagation of the optical ray. However, since light under geometrical optics approximation travels along Fermat's path through a refracting medium, improved quantitative results of the reconstructions are obtained by the use of generalized X-ray tomography algorithms which incorporate correction for refraction.[5]

2. Data gathering and experimental set-up

The experimental set-up is shown in Fig. 1. Light from Laser L, after passing through a combination of static and rotating diffusers (SD and RD), is collimated by lens L_2 and provides illumination to the object, a multimode fibre immersed in toluene of refractive index 1.493 at 0.633 μ. We have used two different samples of graded-index fibres as test objects. For the first $n_{core} = 1.51$ and $n_{cladding} = 1.4805$. For the second fiber, $n_{core} = 1.45$ and $n_{cladding} = 1.44$. The microscope objective (O) mounted on a translation stage is used to image plane E onto the CCD array at the image plane I which is connected to a computer. Designating plane E as the $z = 0$ plane, we gathered two intensities $I(x, y, z = 0)$ and $I(x, y, z = \Delta z)$ corresponding to plane E and one adjacent to it at $z = \Delta z$, where Δz was typically of the order of 200 microns. From these two intensities, $\partial I/\partial z$ is approximated as $[I(x, y, 0) - I(x, y, \Delta z)]/\Delta z$. In the case of

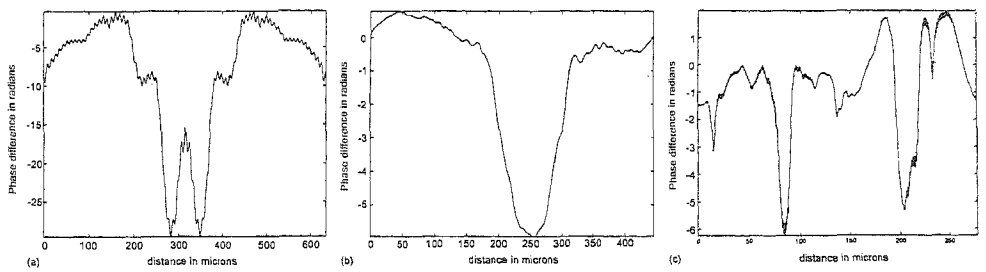

FIG. 2. Phase reconstructed from intensity measurements at plane E of Fig. 1, when TIE is solved using Fourier harmonic expansion. (a) first fibre, (b) second fibre and (c) third object (three-fibre arrangement).

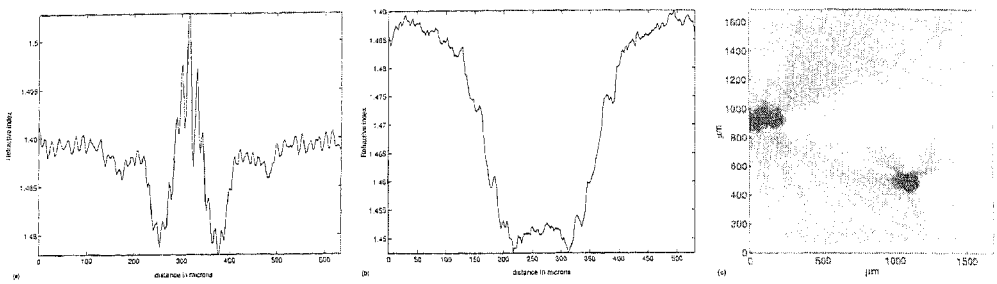

FIG. 3. Reconstructed cross-sections of the test objects. (a) first fibre, (b) second fibre and (c) third object.

fibres, only one set of measurements was needed because of radial symmetry. However, in the case of the third test-object which does not have this symmetry (three fibres placed at the vertices of a triangle), we took 36 sets of intensity data covering a range of 180° around it in equal increments.

3. Results

We solved the TIE by (i) reducing it to a Poisson's equation through a uniform intensity assumption which is solved using a digital cosine transform,[6] (ii) using an iterative procedure after converting it into a finite difference equation[7] and (iii) directly using Fourier harmonic expansion. Figure 2 gives the phase reconstructed from the three test objects using method (iii).[8, 9]

We have inverted the above phase delay data using standard CBP algorithm and used it as the first estimate to the iterative loop for refraction correction. Plots through the centre of the refraction-corrected reconstructions of the two fibres are shown in Figs 3(a) and (b), respectively. The reconstructed peak n_{core} are 1.505 and 1.4525 and $n_{cladding}$ 1.48 and 1.446 for the first and second fibres, respectively. The parabolic profile of the core is recovered in these refraction-correlated reconstructions. Figure 3(c) is the cross-section of the three-fibre object.

4. Conclusions

We have described the use of TIE to recover the phase data from intensity measurements. It is observed that the phase reconstructions obtained without the restriction of constant intensity assumption and incorporation of refraction correction in the tomographic reconstruction algorithm yield reconstructions that are more accurate.

The major advantage of the TIE-based phase reconstruction is that the phase obtained is not restricted to principal values and unwrapping, which usually introduces errors, is not needed. The limitation of the TIE is because of paraxial approximation used in deriving it. Hence, the phase reconstructed cannot be accurate and is limited to those objects which are 'weakly refracting'. We do not expect to encounter nonparaxial rays in tomographic data gathering.

References

1. DEVANY, A. J. AND SCHATZBERG, A. The coherent optical tomographic microscope, *Proc. San Diego Conf.*, SPIE, July 1992.

2. ICHIWAKA, K., LOHMANN, A. W. AND TAKEDA, M. — Phase retrieval based on the irradiance transport equation and the Fourier transform method: experiments, *Appl. Opt.*, 1988, **27**, 3433–3436.

3. TEAGUE, M. R. — Deterministic phase retrieval: A Green's function solution, *J. Opt. Soc. Am. A*, 1983, **73**, 1434–1441.

4. KAK, A. C. AND SLANEY, M. — *Principles of computerized tomographic imaging*, IEEE Press, 1988.

5. LIRA, I. H. AND VEST, C. M. — Refraction correction in holographic interferometry and tomography of transparent objects, *Appl. Opt.*, 1987, **26**, 3919–3928.

6. GHIGLIA, D. C. AND ROMERO, L. A. — Robust two-dimensional weighted and unweighted phase unwrapping that uses fast transforms and iterative methods, *J. Opt. Soc. Am. A*, 1994, **11**, 107–117.

7. VDOVIN, G. — Reconstruction of an object shape from the near-field intensity of a reflected paraxial beam, *Appl. Opt.*, 1997, **36**, 5508–5513.

8. GUREYEV, T. E., ROBERTS, A. AND NUGENT, K. A. — Phase retrieval with the transport of intensity equation: Matrix solution with use of Zernike polynomials, *J. Opt. Soc. Am. A*, 1995, **12**, 1932–1941.

9. GUREYEV, T. E., ROBERTS, A. AND NUGENT, K. A. — Phase retrieval with the transport of intensity equation. II Orthogonal series solution for non-uniform illumination, *J. Opt. Soc. Am. A*, 1996, **13**, 1670–1682.

Thesis Abstract (M. Sc. (Engng))

Segmentation and parameter assignment in constructing continuous model from discrete representation by Arpan Biswas

Research supervisor: Prof. G. Gurumoorthy

Department: Mechanical Engineering

1. Introduction

This work deals with the problem of constructing the continuous/smooth representation of a solid from its discrete representation. Representation in the form of point and mesh of triangles is referred to as discrete representation of the solid. Three steps are involved in constructing the continuous representation. The first involves the grouping of points (given point representation) or triangle (given tessellated representation) in such a way that an appropriate single surface can be fitted to the points/triangles grouped. In the second step, a surface (usually parametric surface) is fitted through the grouped points or the vertices of the grouped triangles. In the last step, the connectivity between the different surfaces obtained is identified and the faces, edges and vertices are generated. The problem of grouping the triangles for an optimized polyhedral representation has been addressed first. A mesh that contains only as many triangles as are necessary to represent the underlying geometry within a specified tolerance is referred to as optimized mesh. The second problem involves the parameterization of the unordered points for interpolating B-spline surface.

2. Segmentation

Optimized polyhedral representation is becoming very common in today's industry. In this work, an algorithm has been proposed for automatically grouping an optimized mesh into its

underlying surfaces. Optimized mesh is associated with a distinct characteristic that is the error value based on which it has been optimized.

To the best of our knowledge no effort has been reported addressing the problem of segmentation in optimized mesh. While detection of the differential property of a surface is more difficult with optimized mesh, the error of tessellation used in generating the optimized mesh is available. The approach presented here utilizes this information to segment the optimized mesh.

2.1. *Procedure of segmentation*

Grouping starts arbitrarily from one triangle and triangles are added incrementally to that group. The decision to add a triangle or not is made based on two criteria, the first one is the inner angle between the normals of the two triangles incident at a common edge and the second one is the chord height error involved in grouping two triangles across their common edge. The chord height error is defined as the maximum deviation between a curve on a smooth surface and its linear approximation generated from the polyhedral representation of the surface.

This chord height error is estimated by passing a curve across the edges of the triangles. Geodesic curve has been used for this purpose and is selected as it is easy to trace and captures the local normal curvature of the surface. The decision about segmentation is taken based on the estimated error and the known error of tessellation.

2.2. *Results*

Two example solids have been used for the validation of the algorithm. These solids contain some typical surface characteristics which are common in engineering objects. Figure 1 shows the outer cylindrical surfaces segmented by the algorithm. Figure 2 shows that the triangles corresponding to the concave region in the periphery are grouped correctly.

3. Parameterization

This work also addresses the problem of initial parameterization of the unordered points for fitting the B-spline parametric surface. The surface calculation procedure is an iterative one. Parameterization of points is necessary to provide an initial guess for the subsequent iterations. A good initial guess is highly desirable for obtaining a good result in the subsequent steps. Two distinct approaches have been proposed in this work for assigning parameter values to points.

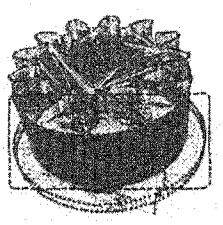

FIG. 1.

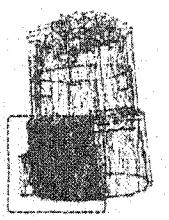

FIG. 2.

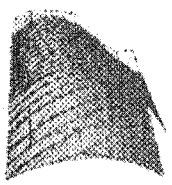

FIG. 3.

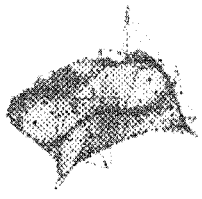

FIG. 4.

3.1. *Literature review*

The schemes proposed by Ma and Kruth[1] and Eck and Hoppe[2] are the most significant works in this area. Ma and Kruth's work[1] is interactive in nature and the success depends largely on the decision of the user. The method proposed by Eck and Hoppe[2] is suitable for a general surface but this is too complicated for a simple surface which is homeomorphic to a circular disc.

3.2. *Parameterization*

In the first approach, parameterization is done by projecting the points on a suitable planar base surface, that is selected automatically. This approach has been implemented for the class of nonwraparound surfaces. The second approach works on a mesh of points. In this approach, the mesh is considered as a spring system. The parametric values are calculated by energy minimization of the spring system.

3.3. *Results*

The surface shown in Fig. 3 has been generated by parameterization with planar base surface method, whereas the surface in Fig. 4 has been generated with the spring-based method. The parameterization based on planar base surface is suitable for nonwraparound surface whereas the spring-based scheme can handle any surface that is homeomorphic to a circular disc.

References

1. MA, W. AND KRUTH, J. P. Parameterization of randomly measured points for least square fitting of B-spline curves and surfaces, *Computer Aided Design*, 1995, **27**, 663–675.

2. ECK, M. AND HOPPE, H. Automatic reconstruction of B-spline surfaces of arbitrary topological type, *Computer Graphics*, 1996, **30**, 325–334 (*SIGGRAPH '96 Proc.*).